Roof stability in deep rock tunnels

Dowon Park[a] and Radoslaw L. Michalowski[a,b]

Abstract

A method is presented addressing quantitative assessment of tunnel roof stability, based on the kinematic approach of limit analysis. Long tunnels with both rectangular (flat-ceiling) and circular cross-sections are considered. The rock is governed by the Hoek-Brown strength envelope and the normality flow rule, and it is assumed to provide enough ductility at failure, making plasticity theorems applicable. A failing block in the collapse mechanism is separated from the stationary rock by a deformation band with a large gradient of velocity across its width. The shape of the block in the critical mechanism is found from the requirement of the mechanism's kinematic admissibility and an optimization procedure consistent with respective measures of stability. The stability number and the supporting pressure needed for tunnel stability are calculated first. Although less commonly used in rock engineering, a procedure is developed for estimating the factor of safety, defined as the ratio of the rock shear strength determined from the Hoek-Brown criterion to the demand on the strength. Curiously, for flat-ceiling tunnels, such definition of the factor of safety yields results equivalent to the ratio of a dimensionless group dependent on the uniaxial compressive strength and the size of the tunnel to the stability number. Such an equivalency does not hold for tunnels with ceilings of finite curvature. Not surprisingly, all measures of tunnel roof stability are strongly dependent on the Geological Strength Index that describes the quality of the rock.

Keywords:

Tunnel roof stability, Hoek-Brown strength criterion, Limit Analysis, Strength reduction factor

[a] Department of Civil & Environmental Eng., University of Michigan, Ann Arbor, U.S.A.

[b] Corresponding author, rlmich@umich.edu

1. Introduction

Roof collapse is a common type of failure[1] in tunnels both during construction and service. An early attempt at an assessment of tunnel roof stability was presented by Lippmann[2] in 1971. His approach included both the kinematic and static approach of limit analysis applied to the rock described by the classical pressure-dependent (Mohr-Coulomb) strength criterion. Davis et al.[3] considered undrained stability of a tunnel roof in clays as well as the face stability during tunnel construction. The latter was also studied by Leca and Dormieux[4] and others[5], but an analysis of this failure type is not carried out in this paper. The interest in stability of tunnels has been increasing as a result of an increasing number of tunneling projects around the world; analytical[6-9] and numerical[9-11] modelling efforts have been carried out for assessment of roof stability. In this paper, the focus is placed on the measures for roof stability assessment in tunnels of rectangular (flat-ceiling) and circular cross-sections.

Fraldi and Guarracino[6, 7] suggested analytical solutions utilizing the calculus of variations in the kinematic approach of limit analysis. The variational approach was used to determine the shape of the failing block in the collapse mechanism. Their solutions address roof collapse in both rectangular and circular cross-section tunnels, in rocks with strength governed by the Hoek-Brown criterion. This method gave rise to a series of other papers, for example[12], most of which focused on the shape of the failing block, rather than stability measures, such as the stability number or a factor of safety. The former was considered more recently for rocks with tension cut-off[8], and an effort is made in this paper to address the various stability measures in regard to roof failures in rocks governed by the Hoek-Brown strength criterion. Suchowerska *et al.*[10] analyzed both deep and shallow tunnel roofs using the finite element upper and lower bound method, and displacement finite element analysis. Stability numbers were reported from their studies for rectangular cavities, and they are used in this paper for comparison.

The focus of this paper is on the stability of roofs in deep tunnels in rocks with strength governed by the Hoek-Brown criterion. The depth of tunnels is assumed sufficient to prevent failure propagating to the ground surface. However, a straight-forward extension of the analysis can be used to address the stability of shallow tunnels[13]. Surprisingly, many analyses of roof stability in deep tunnels have focused on the geometry of the failure mechanisms[6, 7, 12], rather than measures of stability[8, 10]. This paper's focus is on three stability measures: the stability number,

support pressure, and the factor of safety. The latter has been used routinely for geomaterials with strength determined by a linear failure envelope, but the use of the safety factor with failure envelopes nonlinear in the first invariant of the stress tensor is intricate[14].

A brief description of the Hoek-Brown strength criterion and the definitions of the measures of stability are provided first, followed by the description of the mechanism, and the details of the kinematic limit analysis. Numerical results are presented in the form of charts and tables.

2. Hoek-Brown failure criterion and measures of stability

Failure of rocks is characterized by non-linear pressure dependency, contrary to the linear friction-type dependency typically used in analyses of soils. Failure envelopes for rock masses were suggested by Hoek and Brown[15] and Johnston[16]. These criteria were developed based on empirical premises, using laboratory tests and field observations. Both criteria were presented as functions of the major and minor principal stresses, and were functions of the compressive strength of intact rock and other material parameters and indices. This makes it complicated finding an explicit analytical expression for the shear strength envelope on the Mohr plane. Therefore, other forms of non-linear failure criteria were introduced[17-23] with analytical representation making an easier implementation in stability analyses. These, however, did not find a wide acceptance in practice, and it is the Hoek-Brown concept that became the preferred criterion in rock mechanics and engineering.

2.1. Hoek-Brown failure criterion

Since its inception in 1980[15], the Hoek-Brown failure criterion has undergone a series of updates, summarized by Hoek and Marinos[24], and its most recent version[25] is briefly sketched in this subsection. The advantage of this function above other criteria is in the direct relationship of the rock strength to the physical state of rock, expressed through a combination of mechanical parameters and indices. The fundamental expression of the Hoek-Brown failure criterion reads[25]

$$\sigma_1' = \sigma_3' + \sigma_{ci}\left(m_b \frac{\sigma_3'}{\sigma_{ci}} + s\right)^a \tag{1}$$

which is similar to the original function[15] with the exception that coefficient *a* replaced the square root; this modification led to qualifying the function in Eq. (1) as the *generalized* Hoek-Brown criterion. For brevity, we will refer to this function as the Hoek-Brown failure criterion. Stresses σ_1' and σ_3' in Eq. (1) are the effective major and minor principal stresses, respectively, and σ_{ci} is the uniaxial compressive strength of the intact rock. Constant m_b is a reduced value of the material constant m_i for intact rocks

$$m_b = m_i e^{\left(\frac{GSI-100}{28-14D}\right)} \tag{2}$$

This is a dimensionless constant (for a given rock) that introduces pressure dependency into the Hoek-Brown criterion. Typical values of m_i for various rocks can be found in Hoek[26]. Constants *a* and *s* are defined as

$$a = \frac{1}{2} + \frac{1}{6}\left(e^{-\frac{GSI}{15}} - e^{-\frac{20}{3}}\right) \tag{3}$$

$$s = e^{\left(\frac{GSI-100}{9-3D}\right)} \tag{4}$$

where *GSI* is the Geological Strength Index that can vary in the range from 5 to 100, and *D* is a factor defining the degree of rock disturbance, which can vary from zero (undisturbed in-situ rock masses) to 1 (very disturbed rock masses). Examples of index *D* for different construction disturbances can be found in Hoek et al.[25]

When no data is available, Hoek[26] has suggested some representative values of m_i for several rock types; for example, $m_i = 7$ for carbonate rocks, such as limestone and marble, $m_i = 10$ for lithified mudstone, siltstone, or shale, and $m_i = 25$ for course-grained igneous rocks, such as gabbro or granite. In this study, computations of stability measures for tunnel roofs are performed

for a variety of rock types with a *GSI* ranging from 10 to 100 and m_i in the range from 5 to 25. Throughout all calculations, the rock mass is considered minimally disturbed ($D = 0$).

The Hoek-Brown failure surface in the Haigh-Westergaard space is shown in Fig. 1(a). The surface consists of six curvilinear sections, and its intersection with the octahedral plane is shown in Fig. 1(b). The expression in Eq. (1) describes segment EFGE, which includes all limit stress states that satisfy the principal stress combination $\sigma_1' \geq \sigma_2' \geq \sigma_3'$, typical in most calculations. Because the criterion in Eq. (1) is independent of the intermediate principal stress σ_2', surface EFGE does not intersect axis σ_2' (surface with varying curvature, parallel to σ_2'), and any straight line on this surface, for example F'G', is parallel to axis σ_2'. Lines on surface EFGE that are not parallel to axis σ_2' are not straight lines, and the segments of the cross-section of the failure surface with the octahedral plane, Fig. 1(b), are curvilinear. The curvature of these segments is significant only for small hydrostatic pressure, and it decreases with an increase in $\sigma_1' = \sigma_2' = \sigma_3'$.

A single point on the surface in space $\sigma_1', \sigma_2', \sigma_3'$, Fig. 1(a), is mapped on the vector plane in Fig. 1(c) as three stress circles, each determined by a pair of principal stresses. Point E on the hydrostatic axis ($\sigma_1' = \sigma_2' = \sigma_3'$) in the Haigh-Westergaard space is mapped on the strength envelope in Fig. 1(c) as three stress circles, all reduced to a point at location E*. This point can be interpreted as the triaxial (isotropic) tensile strength σ_t, even if the direct measurement of this property cannot be easily carried out. Strength σ_t is a material property, and is a positive number, but the stress equal to the tensile strength is negative (under compression-positive sign convention). By substituting $\sigma_1' = \sigma_3' = -\sigma_t$ into Eq. (1), the value of σ_t is found to be uniquely related to uniaxial compressive strength σ_{ci} and material constants *s* and m_b

$$\sigma_t = \frac{s\sigma_{ci}}{m_b} \tag{5}$$

Uniaxial tensile strength may or may not be equal to σ_t; this is dependent on the curvature of the strength envelope. Calculations indicated that for rocks with disturbance factor $D = 0$, *GSI* in the range of 10 to 100, and m_i in the 5 to 25 range, the uniaxial tensile strength is always smaller than

the isotropic tensile strength σ_t, but the difference does not exceed 4%, and in most cases, it is a fraction of one percent.

Some analyses of stability require that the failure envelope in Fig. 1(c) be given explicitly as a shear strength envelope. For example, most analyses that seek the factor of safety typically require this form. However, a direct transformation of Eq. (1) into an explicit form $\tau = \tau(\sigma_n)$ is cumbersome; consequently, Hoek and Brown[15] suggested an alternative form of the limit state condition as

$$\tau = A\sigma_{ci}\left(\frac{\sigma_n + \sigma_t}{\sigma_{ci}}\right)^B \tag{6}$$

which can be conveniently plotted as an envelope to limit stress circles on the τ-σ_n plane. This form uses two dimensionless material parameters *A* and *B*, in addition to the uniaxial compressive strength of intact rock σ_{ci} and tensile strength σ_t. The reader will notice that by setting *B* = 1, a linear envelope results, and the classical Mohr-Coulomb limit state condition follows when *A* = $\tan\phi$ (ϕ being the internal friction angle). Parameters *A* and *B* can be estimated by matching the envelope in Eq. (6) with stress states in Eq. (1) for a stress range of interest[27].

2.2. Analysis method

The kinematic approach of limit analysis is used in the paper; this method makes an assumption of perfect plasticity, convexity of the failure criterion, and normality of the flow rule. This flow rule implies that strain rate vectors $\dot{\boldsymbol{\varepsilon}}$ in the conjugate space [illegible] are perpendicular to the failure surface in $\sigma_1', \sigma_2', \sigma_3'$ space, as illustrated in Fig. 1(a). Similarly, the velocity discontinuity vectors $\boldsymbol{v}$ on the conjugate plane (with coordinates v_t and v_n), Fig. 1(c), are normal to the strength envelope on plane τ, σ_n. Angle δ will be referred to as the rupture angle[14, 23]. Velocity discontinuities in this approach are interpreted as bands of plastically deforming material with large velocity gradients in the transverse direction[28]. Perfect plasticity implies ductility of deformation, whereas most bonded geomaterials are characterized by some brittle behavior.

Chen[29] argued, however, that if the strain of rock in a boundary value problem is small prior to a brittle drop in stress, then the deformability "may be sufficient to permit the consideration of limit theorems..." Therefore, examples of limit analysis application to rocks can be found throughout the literature[23, 30, 31], including examples of tunnel roof stability[7, 10].

The kinematic theorem of limit analysis allows calculating a rigorous bound to an unknown load (or a different measure of stability) from the balance of work rates of the internal (dissipated) and external work during incipient collapse consistent with a kinematically admissible failure mechanism. The approach yields an upper bound to an active force causing failure, or a lower bound to a reaction (passive force).

2.3. Measures of roof stability

Stability number. One measure of roof stability is a dimensionless combination of the rock properties and the tunnel size, consistent with the tunnel being at the verge of collapse (critical combination). Comparing the actual combination of the parameters for a given tunnel to the critical one allows assessing the safety of the tunnel against the roof collapse. The typical dimensionless group used in the past is the *stability number*, relating the properties of the rock and the size of the tunnel at failure, defined as

$$N = \left(\frac{\sigma_{ci}}{\gamma R} \right)_{crit} \tag{7}$$

where σ_{ci} is the uniaxial compressive strength of intact rock, γ is the unit weight of the rock, and R defines the size of the tunnel (e.g., half-width of rectangular tunnels or a radius of circular tunnels).

Supporting pressure. The critical supporting pressure is defined as the minimum, uniformly distributed traction on the inside surface of the tunnel needed to prevent collapse. The safety margin then follows from comparing the available support stress to the critical one. Support pressure is a passive load, i.e., it is the capacity of the support structure to react to the rock load.

Factor of Safety. This measure of safety is used routinely in soil engineering, but less so in rock engineering. It is typically defined as the ratio of the available shear strength of the geomaterial to the demand on the shear strength. While application of this definition is straightforward for soils governed by the classical Mohr-Coulomb strength envelope, calculations

of the factor of safety for rock structures governed by the Hoek-Brown strength criterion are more intricate.

All three measures of tunnel roof stability will be examined for flat-ceiling and circular-arch roofs.

3. Failure mechanism

Both rectangular and circular cross-section tunnels are illustrated in Fig. 2. The strength of the surrounding rock is described by the Hoek-Brown failure criterion in Eq. (1), and its deformation is governed by the normality plastic flow rule. Possible anisotropy and heterogeneity of the rock is ignored. No distinct joints are assumed to be present in the rock mass. Only deep tunnels are considered, where the loads on the ground surface do not affect the stability of the tunnel, and the roof collapse does not propagate to the ground surface ($H >> h$). However, collapse mechanisms of the type considered in the paper, can be easily generalized for both deep and shallow tunnels, as indicated recently by Fraldi et al.[13]

The tunnels considered are long and the plane-strain analysis will be carried out. The driving force of the roof collapse is the gravity load, and a block moving downward, of yet unknown shape, is the predominant failure mechanism.

Earlier kinematic limit analyses for materials with nonlinear strength criteria[20, 21] included replacement of the geomaterial with a substitution material governed by the classical Mohr-Coulomb envelope tangent to the nonlinear strength criterion. The locus of the point of tangency of the linear approximation and the nonlinear criterion was then one of the variables in the procedure for finding the best bound to a stability/safety measure. The disadvantage of such a method is in an overestimation of the rock strength by the substitution material and in limiting the collapse mechanisms to those with only one rupture angle, often leading to unrealistic failure patterns[2]. The method in this paper utilizes the entire range of rupture angles δ as determined by the normality flow rule and illustrated in Fig. 1(c), thereby increasing the range of admissible failure mechanisms. The tunnel may or may not require supporting pressure p for stability (support pressure p is illustrated in Fig. 2).

The failure mechanisms of a tunnel roof are illustrated for a rectangular-section tunnel and for the circular tunnel in Figs. 3(a) and 3(b), respectively. The piece-wise linear surface $B_0B_jB_{n+1}$

separates the stationary rock from the moving block, and will be referred to as a deformation band, rupture band, or rupture surface. This is a band of plastically deforming material with a large velocity gradient across its width, and it is idealized in calculations as a layer of zero thickness[28] (a kinematic discontinuity). The entire block moves with uniform vertical velocity $\boldsymbol{v}$. Interpreted as a deformation band, rupture layer $B_1B_jB_{n+1}$ undergoes shear and volumetric deformation, with the velocity discontinuity components of v_t and v_n, Fig. 1(c). The rate of volumetric deformation is large in the tensile regime, but it drops with an increase in the compressive stress. This variable volumetric deformation rate is a consequence of nonlinearity of the strength envelope and the normality of the flow rule enforced in limit analysis. The approach taken yields rigorous bounds to stability measures, even if the physical deformation of the rock is not well predicted by the normality flow rule[32].

After initial plastic deformation, band $B_1B_jB_{n+1}$ will form a symmetric half of the detachment surface of the polygon-shaped rock block. However, only incipient failure is considered in limit analysis. The shape of the block is fully defined by n angles α_j, and n-1 angles η_j (and angle β for circular tunnels). Rupture angle δ_j for any segment of the deformation band L_j is related to the shape of the block through independent variable inclination angles α_j as in the following formula

$$\delta_j = \frac{\pi}{2} - \alpha_j \tag{8}$$

This rupture angle relates the specific traction vector on the strength envelope in Fig. 1(c) to every segment L_j of the deformation band. The normal and shear components of the traction vector for an arbitrary point on the strength envelope can be found following Balmer[33] as shown by Kumar[34]

$$\sigma_n = \sigma_{ci}\left\{\left(\frac{1}{m_b} + \frac{\sin\delta}{m_b a}\right)\left[\frac{m_b a\left(1-\sin\delta\right)}{2\sin\delta}\right]^{\frac{1}{1-a}} - \frac{s}{m_b}\right\} \tag{9}$$

$$\tau = \sigma_{ci}\left\{\frac{\cos\delta}{2}\left[\frac{m_b a\left(1-\sin\delta\right)}{2\sin\delta}\right]^{\frac{a}{1-a}}\right\} \tag{10}$$

Equations (9) and (10) constitute a parametric form of the Hoek-Brown strength envelope, instrumental in the analysis.

4. Stability analyses

4.1. Stability number

The rate of internal (dissipated) work in one symmetric half of the tunnel during incipient collapse is computed as integrated rates along all segments of the deformation band

$$D = v\sum_{j=1}^{n}\left(\tau_j \cos\delta_j - \sigma_{nj}\sin\delta_j\right)L_j \tag{11}$$

where v is the magnitude of block velocity vector $\boldsymbol{v}$, L_j is the length of j^{th} segment of the deformation band, and σ_{nj} τ_j are given in Eqs. (9) and (10), with δ_j determined for every segment from Eq. (8). The rate of work done by the rock weight in one half of the tunnel during the tunnel collapse is

$$W_\gamma = \gamma v\left(\sum_{j=1}^{n} S_j - K\right) \tag{12}$$

where S_j is the area of j^{th} triangle $OB_jB_{j+1}O$ in Fig. 3, and

$$K = \frac{R^2}{2} \qquad \text{rectangular tunnel} \tag{13a}$$

$$K = \left(\frac{\pi}{2} - \beta\right)R^2 \qquad \text{circular tunnel} \tag{13b}$$

Requiring a balance of internal (dissipated) and external work rates

$$D = W_\gamma \tag{14}$$

the critical value of the dimensionless group $\sigma_{ci}/\gamma R$ (stability number in Eq. (7)) can be derived as

$$N = \frac{\sigma_{ci}}{\gamma R} = \frac{\sum_{j=1}^{n} S_j - K}{R\sum_{j=1}^{n}\left\{\frac{\cos^2\delta_j}{2}\left[\frac{m_b a\left(1-\sin\delta_j\right)}{2\sin\delta_j}\right]^{\frac{a}{1-a}} - \left[\left(\frac{1}{m_b}+\frac{\sin\delta_j}{m_b a}\right)\left(\frac{m_b a\left(1-\sin\delta_j\right)}{2\sin\delta_j}\right)^{\frac{1}{1-a}} - \frac{s}{m_b}\right]\sin\delta_j\right\}L_j} \tag{15}$$

where K is given in Eqs. (13a) and (13b) for the rectangular and circular cross-section, respectively. The kinematic approach of limit analysis yields the lower bound to stability number N in Eq. (15), and its critical (maximum) value is found through an optimization procedure with the geometry of the block being varied. The details of the process will be given in Section 5.

4.2. Supporting pressure

Safety of tunnels against roof collapse can be improved using rock bolts, or by providing support to the interior tunnel surface (for example, structural tunnel lining). This section considers the minimum support stress the tunnel lining has to withstand to assure stability. Because the supporting stress is a reaction to the rock mass loading, the kinematic approach of limit analysis provides the lower bound to the "pressure" that prevents collapse. This supporting pressure, p, is assumed to be uniformly distributed (Fig. 2). Once support pressure p is incorporated into the collapse mechanisms in Fig. 3, its work rate during an incipient collapse (in one half of the roof failure mechanism) can be calculated easily as

$$W_p = -pvM \tag{16}$$

where

$$M = R \qquad \text{rectangular tunnel} \tag{17a}$$

$$M = R\cos\beta \qquad \text{circular tunnel} \tag{17b}$$

Note that this work is negative, as the supporting pressure is a reaction to the rock mass loading. To find the lower bound to p, the work rate balance in Eq. (14) needs to be amended on the right-

hand side by the term in Eq. (16). Consequently, the dimensionless supporting pressure for the rectangular and circular tunnels can be calculated as

$$\frac{p}{\gamma R}=\frac{1}{RM}\left(\sum_{j=1}^{n}S_j-K\right)-\frac{\sigma_{ci}}{\gamma R}\frac{1}{M}\sum_{j=1}^{n}\left\{\frac{\cos^2\delta_j}{2}\left[\frac{m_b a\left(1-\sin\delta_j\right)}{2\sin\delta_j}\right]^{\frac{a}{1-a}}\right.$$
$$\left.-\left[\left(\frac{1}{m_b}+\frac{\sin\delta_j}{m_b a}\right)\left(\frac{m_b a\left(1-\sin\delta_j\right)}{2\sin\delta_j}\right)^{\frac{1}{1-a}}-\frac{s}{m_b}\right]\sin\delta_j\right\}L_j \tag{18}$$

where K is given in Eqs. (13a) and (14b), and M in Eqs. (17a) and (17b). The dimensionless group $\sigma_{ci}/\gamma R$ represents the actual combination of the rock compressive strength and the tunnel geometry, and it is not its critical value (stability number). If this dimensionless group is larger than the stability number in Eq. (15), no support pressure is necessary.

4.3 Factor of safety

For structures involving soils, the factor of safety is commonly defined as the ratio of shear strength τ of the soil to shear strength τ_d necessary to maintain limit equilibrium (shear strength demand). The same definition is adopted here for rocks, with the exception that the strength is now governed by the Hoek-Brown criterion

$$F=\frac{\tau}{\tau_d} \tag{19}$$

Application of the factor of safety so defined for a linear strength envelope is straightforward, but using this definition with a nonlinear envelope, such as the Hoek-Brown criterion, is not common and is more intricate[14].

The upper curve in Fig. 4 is the Hoek-Brown strength envelope $\tau=\tau(\sigma_n)$, whereas the lower curve represents the reduced shear strength $\tau_d=\tau(\sigma_n)/F=\tau_d(\sigma_n)$. It can be easily shown

that the rupture angle δ at a given point on the Hoek-Brown criterion is associated with the rupture angle δ_d on the reduced-strength envelope through the following relationship (Fig. 4)

$$\delta = \arctan\left(F \tan \delta_d\right) \tag{20}$$

Application of the factor of safety in kinematic limit analysis requires the construction of a failure mechanism in the material with shear strength reduced by factor *F*. Factor *F* will be referred to occasionally as the *strength reduction factor*, and its minimum value is the factor of safety as defined in Eq. (19). Consequently, in calculations of the factor of safety, rupture angles δ on all segments of the rupture surfaces (idealized deformation bands) in Figs. 3(a) and 3(b) need to be replaced with reduced angles δ_d. The reduced angle δ_{dj} on the j^{th} segment of the rupture surface is related to independent variable angle α_j through an equation analogous to Eq. (8). Components σ_{nd} and τ_d of the traction vector on the rupture surface in the material with reduced strength can be calculated now by modifying Eqs. (9) and (10)

$$\sigma_{nd} = \sigma_n = \sigma_{ci}\left\{\left(\frac{1}{m_b} + \frac{\sin\delta_j}{m_b a}\right)\left[\frac{m_b a\left(1-\sin\delta_j\right)}{2\sin\delta_j}\right]^{\frac{1}{1-a}} - \frac{s}{m_b}\right\} \tag{21}$$

$$\tau_d = \frac{\tau}{F} = \frac{\sigma_{ci}}{F}\left\{\frac{\cos\delta_j}{2}\left[\frac{m_b a\left(1-\sin\delta_j\right)}{2\sin\delta_j}\right]^{\frac{a}{1-a}}\right\} \tag{22}$$

where $\delta_j = \arctan(F\tan\delta_{dj})$. Traction components τ, σ_n and τ_d, σ_{nd} with respective rupture angles δ and δ_d are illustrated in Fig. 4 ($\sigma_{nd} = \sigma_n$). The rate of internal (dissipated) work for the symmetric half of the mechanism in the rock with reduced strength can now be found easily from a formula analogous to Eq. (11)

$$D_d = v\sum_{j=1}^{n}\left(\tau_{dj}\cos\delta_{dj} - \sigma_{ndj}\sin\delta_{dj}\right)L_{dj} \tag{23}$$

where σ_{ndj} and τ_{dj} are the traction vector components expressed in Eqs. (21) and (22) for the respective j^{th} segment of the rupture band, and L_{dj} is the length of the segment.

As per Eq. (14), it is now required that the rate of the internal work in Eq. (23) be balanced with the rate of external work, Eq. (12), for the mechanism in the rock with reduced strength. Consequently, the following equation was developed

$$\frac{\sigma_{ci}}{\gamma R}\sum_{j=1}^{n}\left\{\frac{\cos\delta_j}{2F}\left[\frac{m_b a\left(1-\sin\delta_j\right)}{2\sin\delta_j}\right]^{\frac{a}{1-a}}\cos\delta_{dj}-\left(\frac{1}{m_b}+\frac{\sin\delta_j}{m_b a}\right)\left[\frac{m_b a\left(1-\sin\delta_j\right)}{2\sin\delta_j}\right]^{\frac{1}{1-a}}\sin\delta_{dj}+\frac{s}{m_b}\sin\delta_{dj}\right\}L_{dj}=\frac{1}{R}\left(\sum_{j=1}^{n}S_{dj}-K\right) \tag{24}$$

where $\delta_j=\arctan(F\tan\delta_{dj})$, $\sigma_{ci}/\gamma R$ is the actual combination of the rock properties and tunnel geometry, and L_{dj} and S_{dj} are the geometrical quantities in the mechanism with reduced strength (see Fig. 3). Once the set of independent variable angles α_j (j = 1,2...n) in the mechanism of failure is selected, the respective angles δ_{dj} in Eq. (24) are defined by Eq. (8). Eq. (24) is an implicit equation with respect to the strength reduction factor F and it can be solved iteratively (for a set of given angles α_j and η_j). Kinematic limit analysis yields an upper bound to factor of safety F, and it is found by minimizing the strength reduction factor with a variable set of angles α_j and η_j (and β for circular tunnels). A comment on the process of optimization will be included in Section 5.

Calculations can be carried out using Eq. (24) for both the rectangular and circular tunnels, though there is a simpler method that can be used for rectangular (flat-ceiling) tunnels. It is somewhat peculiar that the rate of work dissipation for the mechanism spanning the width of a flat-ceiling tunnel is independent of whether the mechanism is constructed for the true or the reduced rock failure criterion (Fig. 4). Consider two failing blocks in Fig. 5, one for given shear strength $\tau(\sigma_n)$ with the rock rupture along the dashed line, and one in a rock with reduced strength $\tau(\sigma_n)/F$ (solid line). Both are similar to the mechanism in Fig. 3(a), but the rock blocks are now

divided into vertical columns. Based on the geometrical relations in Fig. 5, it can be proved that the dissipation rate calculated from Eq. (11) and Eq. (23) are identical and independent of F

$$D_d = v\sum_{j=1}^{n}\left(\tau_{dj}\cos\delta_{dj} - \sigma_{ndj}\sin\delta_{dj}\right)L_{dj} = v\sum_{j=1}^{n}\left(\tau_j\cos\delta_j - \sigma_{nj}\sin\delta_j\right)L_j = D \tag{25}$$

where subscript d denotes the quantities in the mechanism with reduced failure criterion. It can be further shown that the rate of work of the rock weight in the mechanism with the strength reduced by factor F is equal to that in the mechanism for the true strength criterion decreased by factor F

$$W_{\gamma d} = \frac{1}{F}W_\gamma \tag{26}$$

Consequently, Eqs. (25), (26) and (14) lead to a simple expression for the reduction factor

$$F = \frac{D}{W_\gamma} \tag{27}$$

However, this simple expression cannot be used for circular tunnels, because Eqs. (25) and (26) are valid only for flat-roof tunnels. Further manipulation of Eq. (27) leads to

$$F = \frac{\frac{\sigma_{ci}}{\gamma R}}{N} \tag{28}$$

where the numerator is the dimensionless number for the actual tunnel, and the denominator is the stability number as defined in Eq. (7) and calculated in Eq. (15). Eq. (28) is very useful as it allows calculating the factor of safety for rectangular tunnels in a simple and straightforward manner, without solving the implicit Eq. (24). For reasons of validating this approach, both Eqs. (24) and (28) were used to calculate the factor of safety for flat-ceiling tunnels (both yield identical results). This simpler approach is not applicable to tunnels with arched cross-sections.

5. Results of calculations and discussion

5.1. Optimization of results in limit analysis

The three measures of stability (stability number, required supporting pressure, and the factor of safety) are all calculated based on the mechanisms illustrated in Fig. 3. Surface $B_1B_jB_{n+1}$ is a symmetric half of a band of deforming material, idealized as a zero thickness layer with velocity discontinuity vector $\boldsymbol{v}$ (kinematic discontinuity). This surface is piece-wise linear with n segments, and inclination of segment j^{th} described by independent angle α_j. The length of the j^{th} segment is determined by angles α_j and η_j, as marked in Fig. 3. Preliminary calculations indicated that the rupture surface in rectangular cross-section tunnels always originates at the corners. Consequently, there are n independent angles α_j and $n-1$ independent angles η_j needed to fully describe the shape of the kinematic discontinuity. A circular tunnel requires an additional angle β to describe the shape of the falling block. Angles α_j, η_j and β are independent variables in the optimization process. Kinematic limit analysis provides a lower bound to the stability number and the required supporting pressure (passive load), and the upper bound to the factor of safety. Independent angles α_j and η_j (and β for circular tunnels) were varied with a minimum increment of 0.01°, until a maximum of the stability number or required support pressure was found, or the minimum of the factor of safety was achieved. The calculations were terminated when the difference between two consecutive solutions (dimensionless numbers) was less than 10^{-6}. Because of the symmetry of the problem, calculations were carried out for half of the tunnel. Calculations were carried out with 15 linear segments, $n = 15$ (further increase in n led to negligible improvement of results).

5.2. Stability number

Rectangular tunnels. Stability numbers for rectangular cross-section (flat-ceiling) tunnels, calculated based on Eq. (15), are plotted in Fig. 6, in semi-log scale, as functions of the Geological Strength Index (*GSI*) and parameter m_i. The stability numbers decrease as the *GSI* increases, but they also decrease with a decrease in m_i, which is counterintuitive. Strength index *GSI* has a very

significant effect on the stability number. The numerically obtained results are compared to those based on an analytical procedure that uses limit analysis with a variational approach, suggested by Fraldi and Guarracino[6]. Although Fraldi and Guarracino were more interested in the geometry of the falling block and did not calculate stability numbers, their approach was adopted in the present study to arrive at the results shown as circular bullets in Fig. 6. For all practical purposes, these results are identical to those using the method suggested in this paper. The second set of the results used for comparison comes from the finite element limit analysis, both lower and upper bound, from a paper by Suchowerska et al.[10] The band between lower and upper bound solutions read from the chart in Suchowerska et al.[10] is quite narrow, yet the stability numbers from the approach advocated in this paper plot between the two bounds, as illustrated in Fig. 6. Some numerical values from this study are also given in Table 1.

In the current study, the Hoek-Brown failure criterion in Eq. (1) was used to arrive at the results, whereas the method in the study of Fraldi and Guarracino[6] required the use of explicit approximation $\tau(\sigma_n)$ of the Hoek-Brown envelope. For that purpose, Eq. (6) was used. In calculations of results based on the method of Fraldi and Guarracino, parameters A and B in Eq. (6) were estimated using linear regression suggested by Hoek and Brown[27].

To conclude the comparisons, the shape of the rupture surface is plotted in Fig. 7 for three cases calculated with a different number of segments in the rupture surface. These are compared with the results in Ref.[6] If only one-segment is used in each symmetric half to model the collapse, the shape of the rupture surface noticeably departs from the shape calculated in Ref.[6] However, if ten segments are used, the shape of the roof rupture surface in this study is indistinguishable from that in the analytical approach[6] (corresponding stability numbers are also presented in the figure).

Circular tunnels. Circular cross-section tunnels are common due to the technology used in tunnel construction. The stability numbers of circular tunnels calculated using Eq. (15) are plotted in Fig. 8 in semi-log scale. Not surprisingly, the *GSI* has a very profound influence on the stability number, but for the entire range of *GSI*, the stability numbers are barely distinguishable for different rock types described by constant m_i. For comparative reasons, some numerical values of the stability number for circular tunnels are given in Table 2. When compared to rectangular tunnels in Fig. 6, stability numbers are now far lower for the entire range of *GSI* (and m_i). One plausible reason comes from the effects of the block size. The collapse block in a rectangular tunnel of given width is larger than that during the failure in a circular tunnel of the same width

(the resistance to failure is proportional to the width of the tunnel, whereas the weight of the block increases with the square of the size). Although limit analysis does not allow for calculations of the true stress field, it is possible to inspect the traction (stress vector) on the rupture band in the mechanism used in the analysis. This is because the traction vector is uniquely related to a point on the strength envelope through angle δ. In general, stresses so estimated will not be in equilibrium, but they may indicate some tendencies helpful in explaining the trends in the solutions. The correlation between the distribution of the traction on the rupture surface and the shape of the tunnel (of the same width) is illustrated in Figs. 9(a) and 10(a).

The curves in Fig. 9(a) illustrate the Hoek-Brown strength envelopes for $GSI = 60$ and various m_i, consistent with Eqs. (9) and (10). The bullets on the curves show the dimensionless components of traction vectors on the deformation bands in the critical failure mechanisms (each bullet represents traction components on one of the 15 segments L_j used in the failure mechanisms, Fig. 3). The traction on the deformation band in the neighborhood of the symmetry axis tends to be in the tensile regime, with the compression increasing away from the center plane of the mechanism. It appears that critical mechanisms of roof failure in rectangular tunnels involve traction on the rupture surface in the low range of the normal stress (including the tensile range). Traction vectors on rupture surfaces in circular tunnels span a wider range in compression, providing for larger confining stress and improved stability (lower stability numbers).

The reader will notice that the influence of m_i on the stability of rectangular tunnels (Fig. 6) is more distinct and opposite to that in circular tunnels (Fig. 8). Rocks with a higher value of m_i are likely to be of higher "quality," but, contrary to expectations, the stability number for rectangular tunnels increases with an increase in m_i. A plausible explanation for this peculiarity can be found in the described distribution of the traction vector on the rupture band in the two types of tunnels shown in Fig. 9(a). As described by Hoek-Brown criterion, for a given *GSI*, carbonate rocks described by $m_i = 7$ appear to have larger tensile strength and shear strength in the tensile regime than igneous rocks ($m_i = 25$), while a large portion of the rupture band in flat-ceiling tunnels appears to be subjected to traction in the tensile regime. The opposite trend in stability number with respect to m_i is found for circular tunnels, where traction on the deformation band spans a wider range in compression. While this is a plausible reason for the trends in the stability number, it needs to be emphasized again that traction vector components calculated from the kinematic approach are not true stresses, as the method does not assure equilibrium of the stress

field. The influence of parameter m_i on the shape of rupture surfaces for $GSI = 60$ in the two types of tunnels are illustrated in Figs. 9(b). The influence of GSI on the shape of the failure mechanism for $m_i = 7$ is shown in Figs. 10(b).

Information about the height of the block in the failure mechanisms is presented in the chart in Fig. 11; height h and tunnel size R are illustrated in Fig. 2. Both indices GSI and m_i affect the height of the block, and the rectangular tunnels involve larger (taller) blocks. The height of the block reaches the minimum when the rock's GSI is equal to about 25, and it increases with a decrease in m_i (m_i describes the rock type).

Stability numbers for roofs in circular tunnels in rocks with strength governed by the Hoek-Brown criterion have not been reported earlier, hence the results in Fig. 8 could not be compared to those from other studies. The study of Fraldi and Guarracino[7], for example, focused only on the geometry (shape) of the failing block, and not on any measures of stability. However, even the shape of the block from that study cannot be reliably compared with that in the present study. This is because in Ref.[7] an assumption was made that the shape of the surface separating the moving block from the stationary rock is independent of the tunnel ceiling shape (this was a sound assumption only for flat-ceiling tunnels where the rupture surface always originates from the corners).

5.3. Required supporting pressure

As the kinematic approach yields the lower bound to the supporting pressure (passive load), the required value was calculated by maximizing dimensionless group $p/\gamma R$ in Eq. (18). The results are plotted in Fig. 12. In general, rectangular tunnels characterized by the same dimensionless number of $\sigma_{ci}/\gamma R$ require greater supporting pressure than circular tunnels do.

For circular tunnels, Fig. 12(b), the required support pressure increases with a decrease in m_i, as expected. For rectangular tunnels, however, this trend is true only for larger supporting pressures, Fig. 12(a). The source of this curiosity for flat-ceiling tunnels is likely to be in a low confining stress (or even tensile stress) on the rupture band separating the moving block from the stationary rock. This is confirmed by inspecting the traction vector on the deformation band for tunnels that require a support pressure for stability. The open bullets in Fig. 13 show the components of the traction vector on the deformation band in flat-ceiling tunnels that are at the

verge of collapse. The stability numbers N for these tunnels are 32.65, 38.47 and 46.63 for rocks with m_i equal to 7, 10 and 15, respectively. The filled bullets illustrate the traction vectors for tunnels of twice the width, but in the same rocks. Now the tunnels need a supporting pressure for stability ($p/\gamma R$ equal to 0.187, 0.148 and 0.118 for rocks of $m_i = 7$, 10 and 15, respectively). Introducing the support pressure moves the confining stress on the rupture band into the range where the shear stress of rock increases with an increase in m_i (as in Fig. 13), reversing the trend in Fig. 12(a).

5.4. Factor of safety

Although the stability number is useful in stability assessment of structures, the factor of safety is a more intuitive measure. Based on the approach proposed in this study, the factors of safety for tunnels can be calculated for either flat-ceiling or circular cross-section tunnels from Eq. (24), or from Eq. (28) for rectangular tunnels only. Because the latter provides a straightforward approach for rectangular tunnels (utilizing Eq. (15) or the charts in Fig. 6), computational results for factors of safety will be presented in a chart for circular tunnels, with only limited data for flat-ceiling tunnels in Table 3.

Factors of safety for circular tunnels were calculated from an implicit expression in Eq. (24). They are presented in Fig. 14 as a function of $\sigma_{ci}/\gamma R$ for various rock indices *GSI* and m_i. Numerical values of the factor of safety are given in Table 4 for selected dimensionless group $\sigma_{ci}/\gamma R$ and rock indices. Not surprisingly, the factor of safety increases with an increase in *GSI*, and for given *GSI*, it increases with $\sigma_{ci}/\gamma R$. Because the critical combination of $\sigma_{ci}/\gamma R$ is equal to the stability number as defined in Eq. (7), all values on the horizontal axis for $F = 1$ are equal to stability numbers for the particular combinations of *GSI* and m_i. The Geological Strength Index has a profound influence on the factor of safety.

It is common to consider the factor of safety as a ratio of geomaterial shear strength to the demand on the shear strength needed to avoid collapse, as in Eq. (19). Consequently, it is tempting to define the factor of safety for tunnels as the ratio of dimensionless group $\sigma_{ci}/\gamma R$ to its critical value (stability number N in Eq. (7)). Factors of safety calculated using both the definition in Eq. (28) and the one in Eq. (19) are illustrated in Fig. 15. As predicted earlier, for rectangular cross-section tunnels both definitions yield identical results, but it is a special case that cannot be

generalized. For circular tunnels, the definition in Eq. (28) significantly overestimates the factor of safety based on the shear strength demand, Eq. (19), and calculated from Eq. (24).

5.5. Example

Consider a deep circular tunnel with 5 m radius (R = 5 m), with the following rock mass properties/indices: γ = 26 kN/m^3, σ_{ci} = 20 MPa, GSI = 20, m_i = 5, D = 0 (m_b, a and s are calculated from Eqs. (2) through (4)). The dimensionless group $\sigma_{ci}/\gamma R$ = 153.8, whereas the stability number from Fig. 8 is 108.5. Because this tunnel is stable (the lower the stability number compared to the dimensionless group $\sigma_{ci}/\gamma R$, the more stable the tunnel), no supporting pressure is required. By reading the chart in Fig. 14, the factor of safety can be determined: F = 1.21.

The dimensionless number $\sigma_{ci}/\gamma R$ for a tunnel with radius of 10 m in the same rock mass would be only 76.9, thus lower than stability number 108.5 (factor of safety from Eq. (24) is F = 0.83). A supporting pressure is needed to render the tunnel stable. One can read $p/\gamma R$ = 0.034 for $\sigma_{ci}/\gamma R$ = 76.9 from the chart in Fig. 12(b). The required supporting pressure is then equal to 0.034×γR = 8.84 kPa. This is a lower bound to the pressure needed for limit equilibrium (F = 1). Now, if a factor of safety of F = 2.0 was required, one could calculate the required pressure that assures F = 2.0 by including the work of the supporting pressure in Eq. (16) into the work rate balance in Eq. (14). Given safety factor F, and following the path used to develop Eq. (24), the following expression for the required support pressure is found

$$\frac{p}{\gamma R}=\frac{1}{RM}\left(\sum_{j=1}^{n}S_{dj}-K\right)-\frac{\sigma_{ci}}{\gamma R}\frac{1}{M}\sum_{j=1}^{n}\left\{\frac{\cos\delta_j}{2F}\left[\frac{m_b a\left(1-\sin\delta_j\right)}{2\sin\delta_j}\right]^{\frac{a}{1-a}}\cos\delta_{dj}\right.$$
$$\left.-\left(\frac{1}{m_b}+\frac{\sin\delta_j}{m_b a}\right)\left[\frac{m_b a\left(1-\sin\delta_j\right)}{2\sin\delta_j}\right]^{\frac{1}{1-a}}\sin\delta_{dj}+\frac{s}{m_b}\sin\delta_{dj}\right\}L_{dj} \tag{29}$$

where $\delta_j=\arctan(F\tan\delta_{dj})$. This is an explicit equation for the required dimensionless pressure $p/\gamma R$, because the factor of safety is given. The maximization of the pressure takes place with respect to angles δ_{dj}, η_j and β in the mechanism in Fig. 3(b). Calculations indicated that a supporting pressure of 131.1 kPa is needed to assure a safety factor of 2 (334.5 kPa when the required factor of safety is raised to 3). Notice that setting $p/\gamma R$ = 0, Eq. (29) can be transformed

into the implicit Eq. (24) for calculating the factor of safety, whereas setting $p/\gamma R = 0$ and $F = 1$, Eq. (15) for calculating the stability number is recovered.

6. Conclusions

The kinematic approach of limit analysis was applied to consider stability of roofs in deep tunnels. The collapse mechanism includes a rock block moving downward, separated from the stationary rock by a band of deforming material. The rock in the band was assumed to allow enough ductility to permit application of plasticity theorems. The shape of the block is not predetermined, and it follows from a straightforward yet effective method using the plastic flow rule associated with the Hoek-Brown failure criterion.

Three measures of stability were calculated: the stability number, required supporting pressure, and the factor of safety. In general, the stability number for tunnels of comparable width are smaller for tunnels with a circular cross-section compared to rectangular (flat-ceiling) tunnels (the lower the stability number compared to the dimensionless group $\sigma_{ci}/\gamma R$, the more stable the tunnel). Inspection of the traction vector on the band separating the failing block from the stationary rock revealed that the 'confining pressure' above the tunnel ceiling in circular cross-section tunnels is larger than that in flat-ceiling tunnels (of comparable size), providing for lower stability numbers. Stability numbers are very strongly dependent on the Geological Strength Index (*GSI*), but less so on the type of rock (m_i). The most critical failure mechanisms for rectangular cross-section tunnels include a rock block spanning the entire width of the tunnel roof, and the block is larger than those in circular tunnels of comparable width. In both cases, the height (size) of the block is dependent on the *GSI*, with the smallest block for the *GSI* equal to about 25. The size of the block tends to increase substantially with an increase of parameter m_i, which describes the type of rock.

The definition of the factor of safety adopted here was the ratio of the rock shear strength to the demand on the shear strength assuring the roof is stable. While straightforward for failure envelopes linear in the first invariant of the stress tensor, its application is more elaborate for nonlinear criteria. Calculations require solving an implicit equation, and the details of the specific procedure for calculating the factor of safety for the tunnels with rock strength governed by the Hoek-Brown criterion are described in the paper. Not surprisingly, factors of safety strongly

depend on the dimensionless group that involves the compressive strength of the rock and the size of the tunnel ($\sigma_{ci}/\gamma R$), and for a given $\sigma_{ci}/\gamma R$, it is strongly dependent on the *GSI*. Factors of safety for flat-ceiling tunnels can be alternatively calculated as a ratio of $\sigma_{ci}/\gamma R$ to stability number *N*. This peculiarity is a consequence of the geometry of the failure mechanism in the tunnels with flat ceilings, and cannot be used for tunnels with ceilings of finite radius of curvature.

Acknowledgements

The work presented in this paper was carried out while the authors were supported by the National Science Foundation, Grant No. CMMI-1901582, and the Horace Rackham School of Graduate Studies at the University of Michigan. This support is greatly appreciated.

References

1. Hoek E. *Practical Rock Engineering*: Online. ed. Rocscience; 2007.
2. Lippmann H. Plasticity in rock mechanics. *Int J Mech Sci.* 1971;13(4): 291-297.
3. Davis EH, Gunn MJ, Mair RJ, Seneviratine HN. The stability of shallow tunnels and underground openings in cohesive material. *Géotechnique.* 1980;30(4): 397-416.
4. Leca E, Dormieux L. Upper and lower bound solutions for the face stability of shallow circular tunnels in frictional material. *Géotechnique.* 1990;40(4): 581-606.
5. Saada Z, Maghous S, Garnier D. Pseudo-static analysis of tunnel face stability using the generalized Hoek–Brown strength criterion. *Int J Numer Anal Meth Geomech.* 2013;37(18): 3194-3212.
6. Fraldi M, Guarracino F. Limit analysis of collapse mechanisms in cavities and tunnels according to the Hoek–Brown failure criterion. *Int J Rock Mech Min Sci.* 2009;46(4): 665-673.
7. Fraldi M, Guarracino F. Analytical solutions for collapse mechanisms in tunnels with arbitrary cross sections. *Int J Solids Struct.* 2010;47(2): 216-223.
8. Park D, Michalowski RL. Tunnel roof stability in soft rock with tension cutoff. *GeoShanghai International Conference.* Springer; 2018:361-368.
9. Sloan S, Assadi A. Stability of shallow tunnels in soft ground. *Predict Soil Mech London: Thomas Telford.* 1993: 644-663.
10. Suchowerska AM, Merifield RS, Carter JP, Clausen J. Prediction of underground cavity roof collapse using the Hoek–Brown failure criterion. *Comput Geotech.* 2012;44: 93-103.
11. Abbo AJ, Wilson DW, Sloan SW, Lyamin AV. Undrained stability of wide rectangular tunnels. *Comput Geotech.* 2013;53: 46-59.
12. Yang X, Huang F. Three-dimensional failure mechanism of a rectangular cavity in a Hoek–Brown rock medium. *Int J Rock Mech Min Sci.* 2013;61: 189-195.
13. Fraldi M, Cavuoto R, Cutolo A, Guarracino F. Stability of tunnels according to depth and variability of rock mass parameters. *Int J Rock Mech Min Sci.* 2019;119: 222-229.
14. Michalowski RL. Failure potential of infinite slopes in bonded soils with tensile strength cut-off. *Can Geotech J.* 2017;55(4): 477-485.
15. Hoek E, Brown ET. Empirical strength criterion for rock masses. *Journal of the Geotechnical Engineering Division.* 1980;106(9): 1013-1035.

16. Johnston IW. Strength of intact geomechanical materials. *J Geotech Eng-ASCE.* 1985;111(6): 730-749.
17. Drucker DC, Prager W. Soil mechanics and plastic analysis or limit design. *Q Appl Math.* 1952;10(2): 157-165.
18. Paul B. A modification of the Coulomb-Mohr theory of fracture. *J Appl Mech.* 1961;28(2): 259-268.
19. Zhang X, Chen W. Stability analysis of slopes with general nonlinear failure criterion. *Int J Numer Anal Meth Geomech.* 1987;11(1): 33-50.
20. Drescher A, Christopoulos C. Limit analysis slope stability with nonlinear yield condition. *Int J Numer Anal Meth Geomech.* 1988;12(3): 341-345.
21. Collins IF, Gunn CIM, Pender MJ, Yan W. Slope stability analyses for materials with a non-linear failure envelope. *Int J Numer Anal Meth Geomech.* 1988;12(5): 533-550.
22. Michalowski RL. Stability of intact slopes with tensile strength cut-off. *Géotechnique.* 2017;67(8): 720-727.
23. Park D, Michalowski RL. Three-dimensional stability analysis of slopes in hard soil/soft rock with tensile strength cut-off. *Eng Geol.* 2017;229: 73-84.
24. Hoek E, Marinos P. A brief history of the development of the Hoek-Brown failure criterion. *Soils Rocks.* 2007;2(November): 1-13.
25. Hoek E, Carranza-Torres C, Corkum B. Hoek-Brown failure criterion-2002 edition. *Proceedings of NARMS-Tac.* 1. 2002:267-273.
26. Hoek E. Estimating Mohr-Coulomb friction and cohesion values from the Hoek-Brown failure criterion. *Intnl J Rock Mech & Mining Sci & Geomechanics Abstracts.* 1990;12(3): 227-229.
27. Hoek E, Brown ET. Practical estimates of rock mass strength. *Int J Rock Mech Min Sci.* 1997;34(8): 1165-1186.
28. Drucker D, Prager W, Greenberg H. Extended limit design theorems for continuous media. *Q Appl Math.* 1952;9(4): 381-389.
29. Chen W-F. *Limit analysis and soil plasticity*. New York: Elsevier Scientific Publishing Company; 1975.
30. Michalowski R. Limit analysis of quasi-static pyramidal indentation of rock. *Int J Rock Mech Min Sci.* 1985;22(1): 31-38.

31. Chen WF, Drucker DC. Bearing capacity of concrete blocks or rock. *J Eng Mech Div.* 1969;95(4): 955-978.
32. Radenkovic D. Théorie des charges limites extension a la mécanique des sols. Séminaire de Plasticité. École Polytechnique, Publications Scientifiques et Techniques du Ministère de L'Air; 1962:129-141.
33. Balmer G. A general analysis solution for Mohr's envelope. *Proc ASTM.* 1952;52: 1260-1271.
34. Kumar P. Shear failure envelope of Hoek-Brown criterion for rockmass. *Tunn Undergr Sp Tech.* 1998;13(4): 453-458.

Figure Captions

Figure 1. Hoek-Brown strength criterion: (a) failure surface in Haigh-Westergaard space, (b) cross-section on octahedral plane, and (c) strength envelope on $\tau - \sigma_n$ plane.

Figure 2. Problem geometry (H >> h), including supporting pressure *p*: (a) rectangular (flat-ceiling) tunnel, and (b) circular tunnel.

Figure 3. Schematics of roof collapse mechanisms: (a) rectangular tunnel, and (b) circular tunnel.

Figure 4. Hoek-Brown strength envelope and the strength envelope reduced by factor *F*.

Figure 5. Geometric relations in flat-ceiling tunnel mechanisms for full rock strength and reduced rock strength.

Figure 6. Stability numbers obtained in this study for rectangular tunnels (rock disturbance factor $D = 0$), and comparison with results from Suchowerska *et al*. (2012) and those based on approach of Fraldi and Guarracino (2009).

Figure 7. Comparison of the shape of the rupture surface from this study and Fraldi and Guarracino (2009), and associated stability numbers (*n* – number of linear segments describing the shape of a symmetric half of the block; $GSI = 80$, $m_i = 7$, $D = 0$).

Figure 8. Stability numbers as functions of *GSI* and m_i for circular tunnels ($D = 0$).

Figure 9. The influence of tunnel geometry and m_i ($GSI = 60$, $D = 0$) on the solution: (a) traction vector on the rupture surface, and (b) profiles of collapsing blocks.

Figure 10. The influence of tunnel geometry and *GSI* ($m_i = 7$, $D = 0$) on the solution: (a) traction vector on the rupture surface, and (b) profiles of collapsing blocks.

Figure 11. The height of the failed mass (rock block).

Figure 12. Required supporting pressure: (a) rectangular tunnels, and (b) circular tunnels.

Figure 13. Traction vector on the rupture surface for flat-roof tunnels with and without supporting pressure.

Figure 14. Factors of safety for circular tunnels.

Figure 15. Comparison of factors of safety defined by the shear strength demand, Eq. (19), and uniaxial compressive strength, Eq. (28).

Table 1. Stability numbers for rectangular tunnels ($D = 0$)

GSI	m_i				
	5	10	15	20	25
10	1136.45	1565.30	1900.41	2184.49	2434.90
20	460.87	639.24	777.70	895.10	998.71
30	213.60	296.26	360.49	414.87	462.90
40	105.70	146.28	177.86	204.61	228.27
50	54.00	74.47	90.42	103.96	115.94
60	28.03	38.47	46.63	53.57	59.71
70	14.68	20.02	24.22	27.79	30.96
80	7.73	10.46	12.62	14.47	16.10
90	4.08	5.48	6.60	7.55	8.39
100	2.17	2.88	3.45	3.94	4.38

Table 2. Stability numbers for circular tunnels ($D = 0$)

GSI	m_i				
	5	10	15	20	25
10	299.31	293.68	291.42	289.77	289.47
20	108.58	106.66	105.94	105.45	105.33
30	50.63	49.70	49.34	49.11	49.04
40	26.55	25.99	25.79	25.66	25.62
50	14.71	14.36	14.23	14.14	14.11
60	8.36	8.13	8.04	7.99	7.97
70	4.81	4.66	4.60	4.56	4.55
80	2.78	2.68	2.64	2.62	2.61
90	1.61	1.55	1.52	1.51	1.50
100	0.94	0.90	0.88	0.87	0.86

Table 3. Factors of safety for rectangular tunnels ($D = 0$)

$\sigma_{ci}/\gamma R$	GSI	m_i				
		5	10	15	20	25
5000	10	4.399	3.194	2.631	2.288	2.053
	20	10.848	7.821	6.429	5.585	5.006
500	30	2.340	1.687	1.386	1.205	1.080
	40	4.730	3.418	2.811	2.443	2.190
	50	9.258	6.714	5.529	4.809	4.312
50	60	1.783	1.299	1.072	0.933	0.837
	70	3.405	2.496	2.064	1.798	1.614
	80	6.467	4.776	3.959	3.454	3.104
	90	12.229	9.111	7.575	6.621	5.954
5	100	2.302	1.733	1.446	1.266	1.140

Table 4. Factors of safety for circular tunnels ($D = 0$)

$\sigma_{ci}/\gamma R$	GSI	m_i				
		5	10	15	20	25
1000	10	2.004	1.945	1.922	1.910	1.902
	20	3.790	3.498	3.382	3.319	3.278
100	30	1.458	1.448	1.444	1.442	1.440
	40	2.155	2.082	2.054	2.038	2.029
	50	3.232	3.005	2.912	2.861	2.829
10	60	1.106	1.117	1.121	1.123	1.124
	70	1.549	1.528	1.519	1.514	1.511
	80	2.256	2.149	2.102	2.075	2.058
	90	3.464	3.152	3.013	2.932	2.879
1	100	1.038	1.062	1.071	1.075	1.078

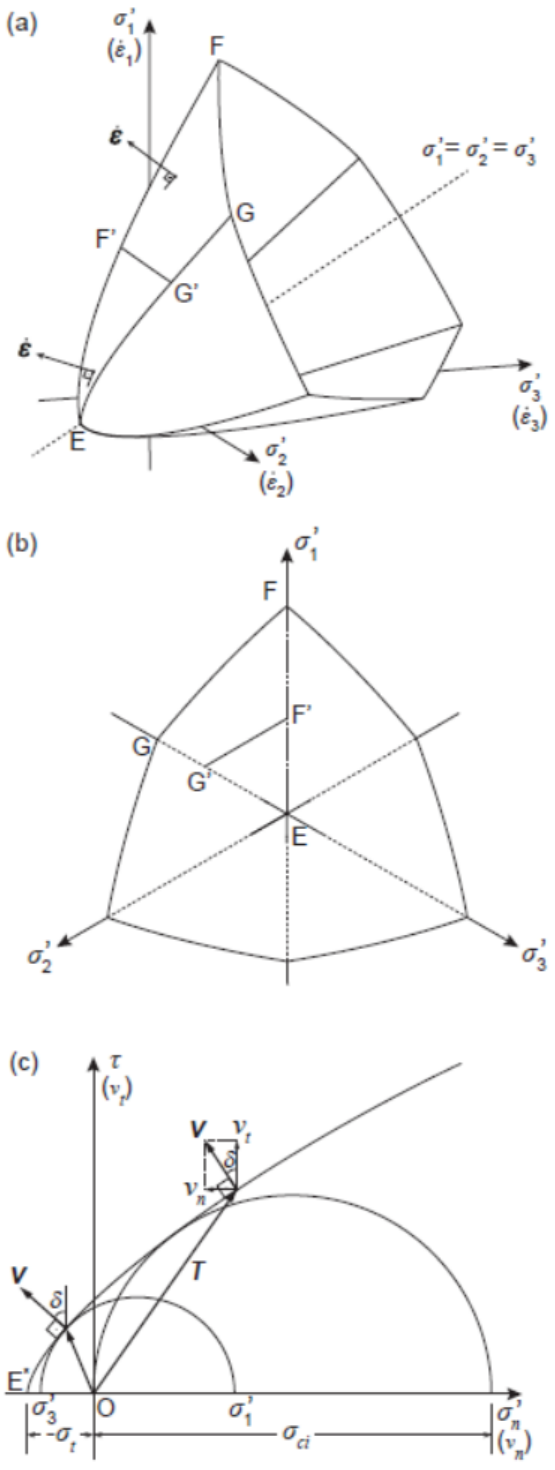
(a)
σ_1'
$(\dot{\varepsilon}_1)$
F
$\dot{\boldsymbol{\varepsilon}}$
$\sigma_1' = \sigma_2' = \sigma_3'$
G
F'
G'
$\dot{\boldsymbol{\varepsilon}}$
σ_3'
$(\dot{\varepsilon}_3)$
E
σ_2'
$(\dot{\varepsilon}_2)$
(b)
σ_1'
F
F'
G
G'
E
σ_2'
σ_3'
(c)
τ
(v_t)
$\boldsymbol{V}$
v_t
v_n
δ
$\boldsymbol{V}$
δ
$\boldsymbol{T}$
E'
σ_3'
O
σ_1'
σ_n'
(v_n)
$-\sigma_t$
σ_{ci}

Figure 1

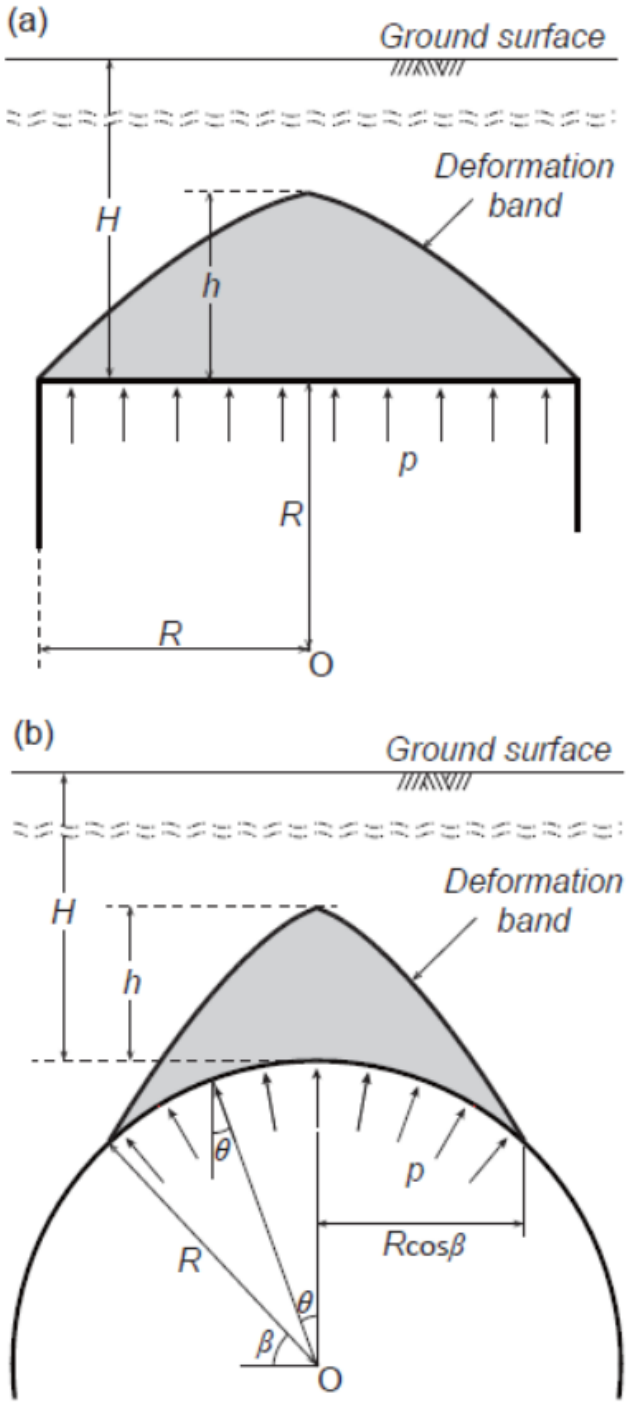
(a)
Ground surface
Deformation band
H
h
p
R
R
O
(b)
Ground surface
Deformation band
H
h
θ
p
Rcosβ
R
θ
β
O

Figure 2

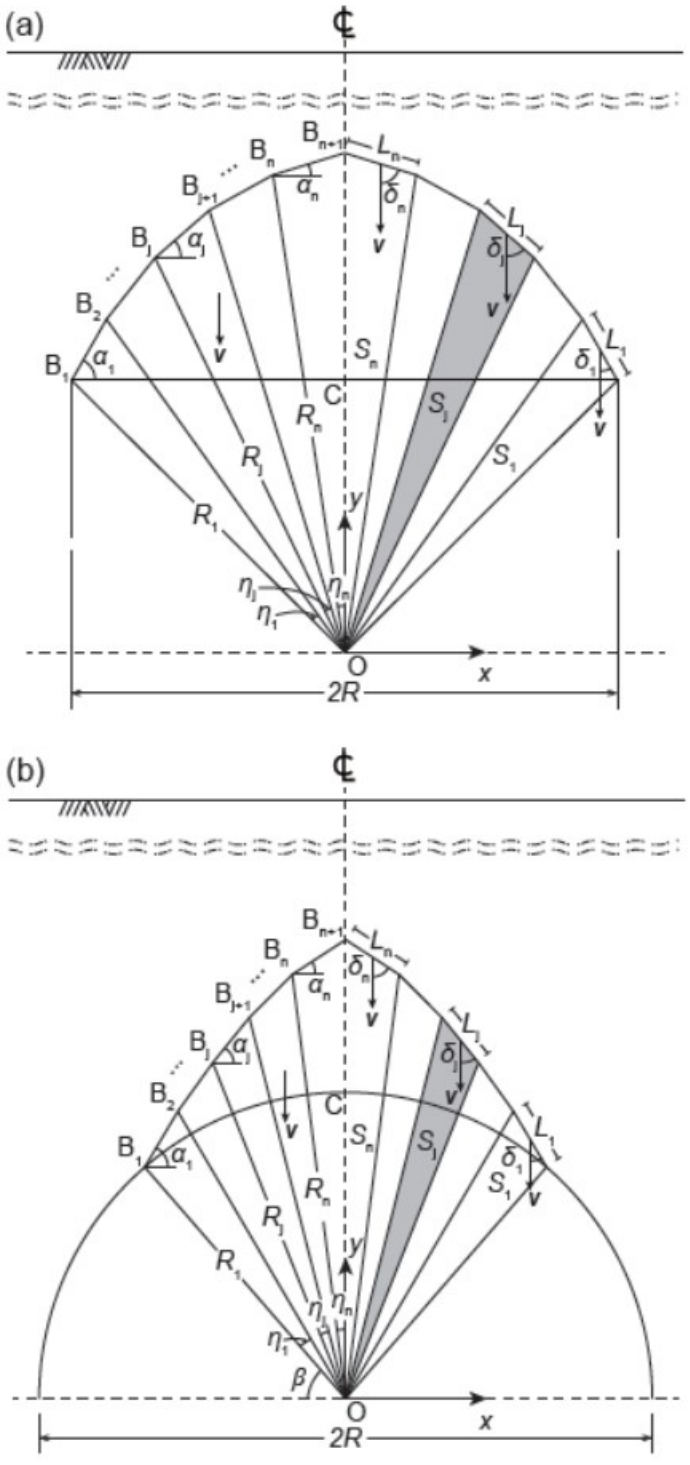

Figure 3

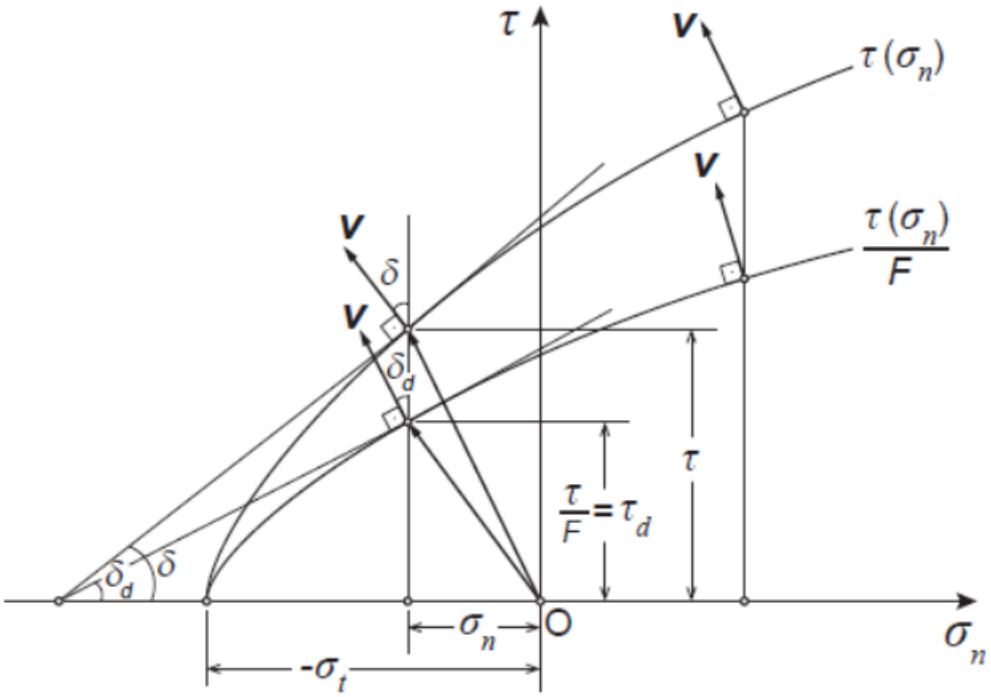

Figure 4

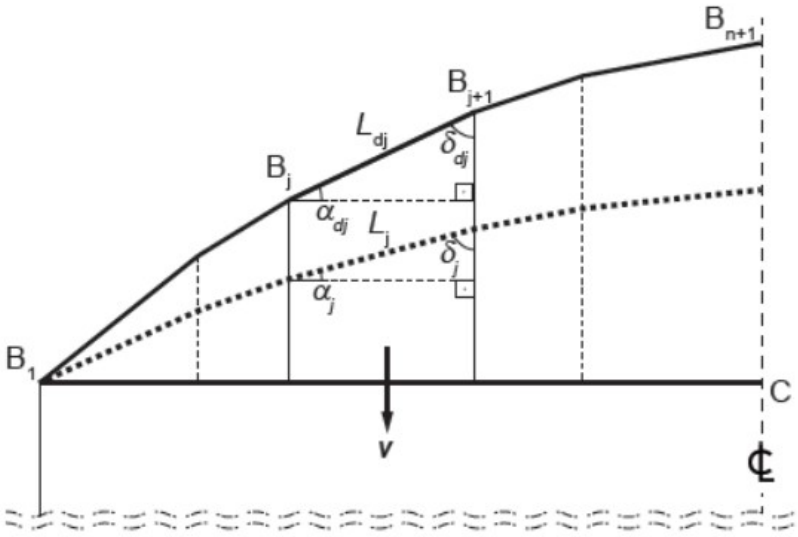

Figure 5

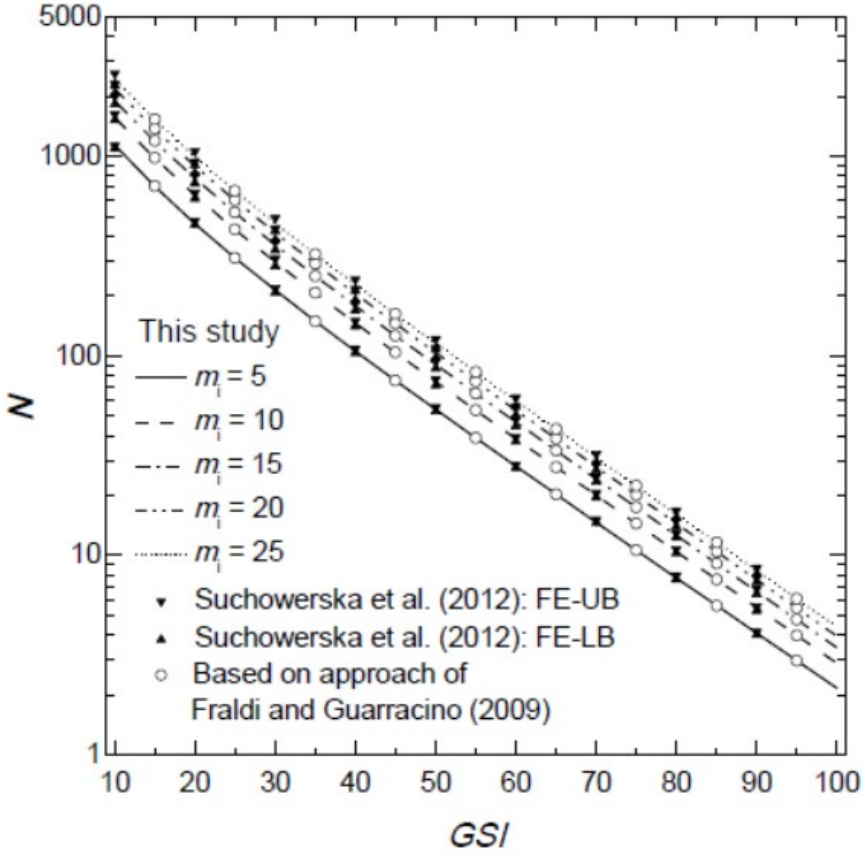
5000
1000
100
10
1
N
10
20
30
40
50
60
70
80
90
100
GSI
This study
m_i = 5
m_i = 10
m_i = 15
m_i = 20
m_i = 25
Suchowerska et al. (2012): FE-UB
Suchowerska et al. (2012): FE-LB
Based on approach of
Fraldi and Guarracino (2009)

Figure 6

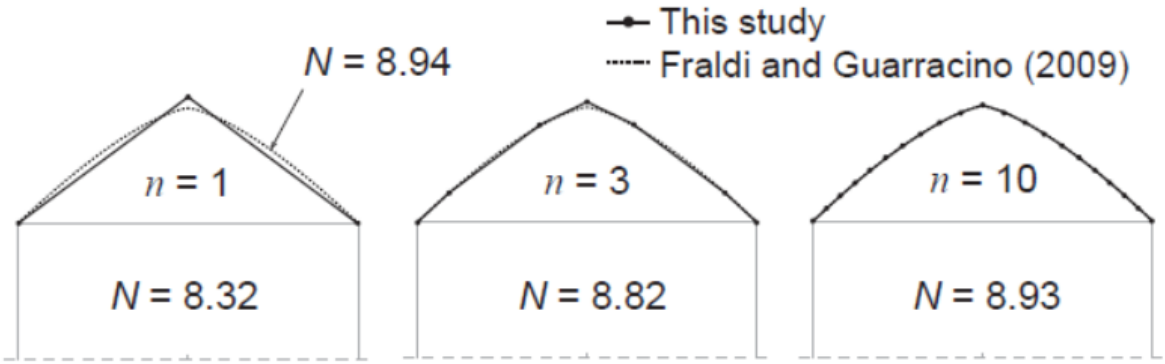
This study
Fraldi and Guarracino (2009)
N = 8.94
n = 1
N = 8.32
n = 3
N = 8.82
n = 10
N = 8.93

Figure 7

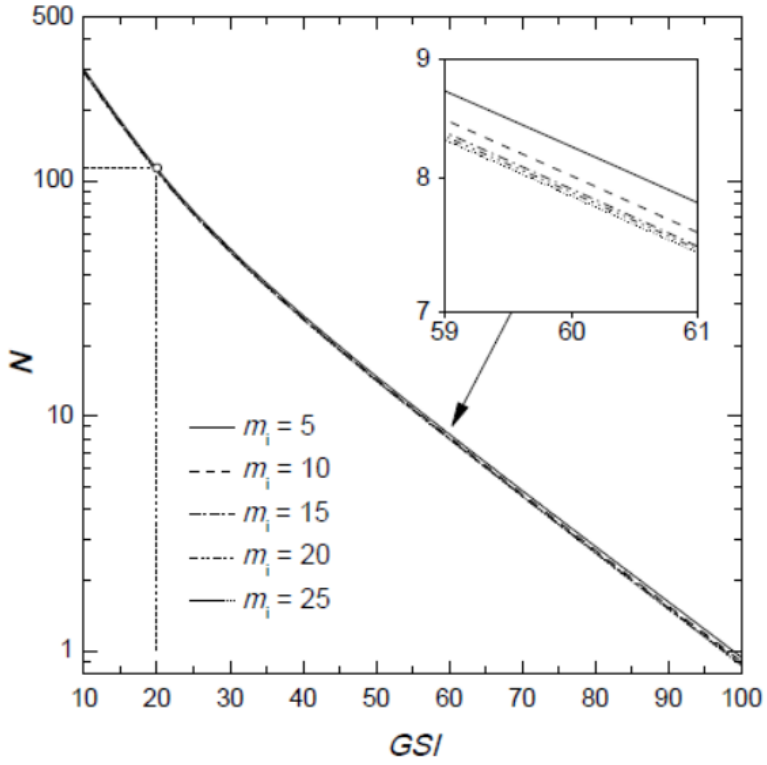
500
100
10
1
N
10
20
30
40
50
60
70
80
90
100
GSI
9
8
7
59
60
61
m_i = 5
m_i = 10
m_i = 15
m_i = 20
m_i = 25

Figure 8

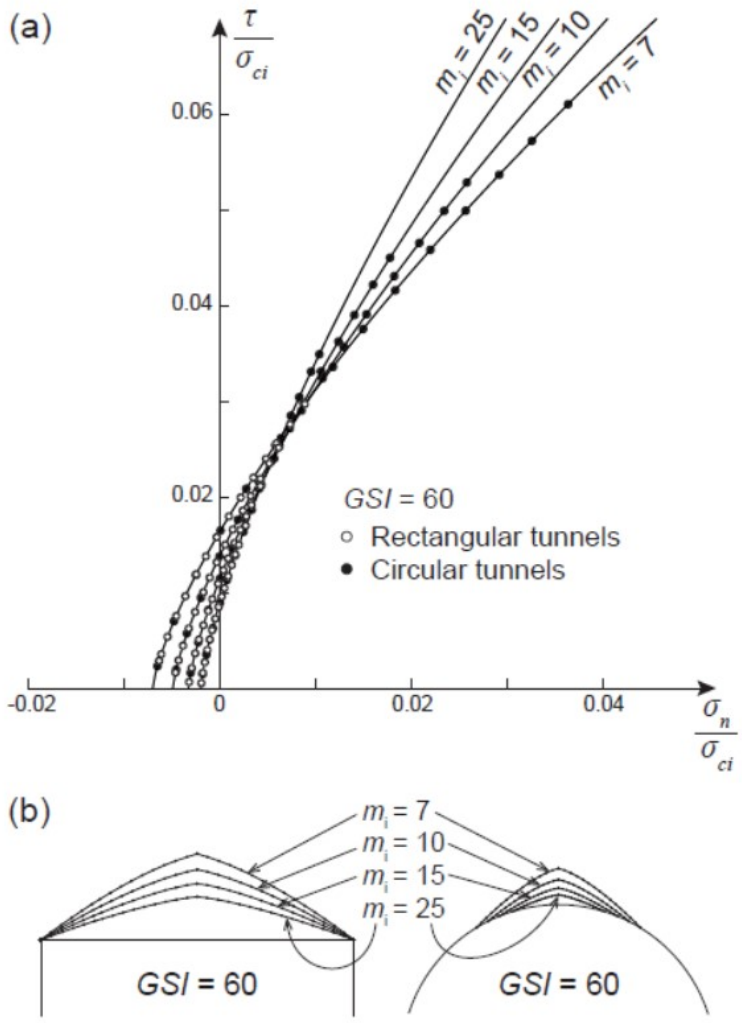
(a)
τ / σci
0.06
0.04
0.02
mi = 25
mi = 15
mi = 10
mi = 7
GSI = 60
Rectangular tunnels
Circular tunnels
-0.02
0
0.02
0.04
σn / σci
(b)
mi = 7
mi = 10
mi = 15
mi = 25
GSI = 60
GSI = 60

Figure 9

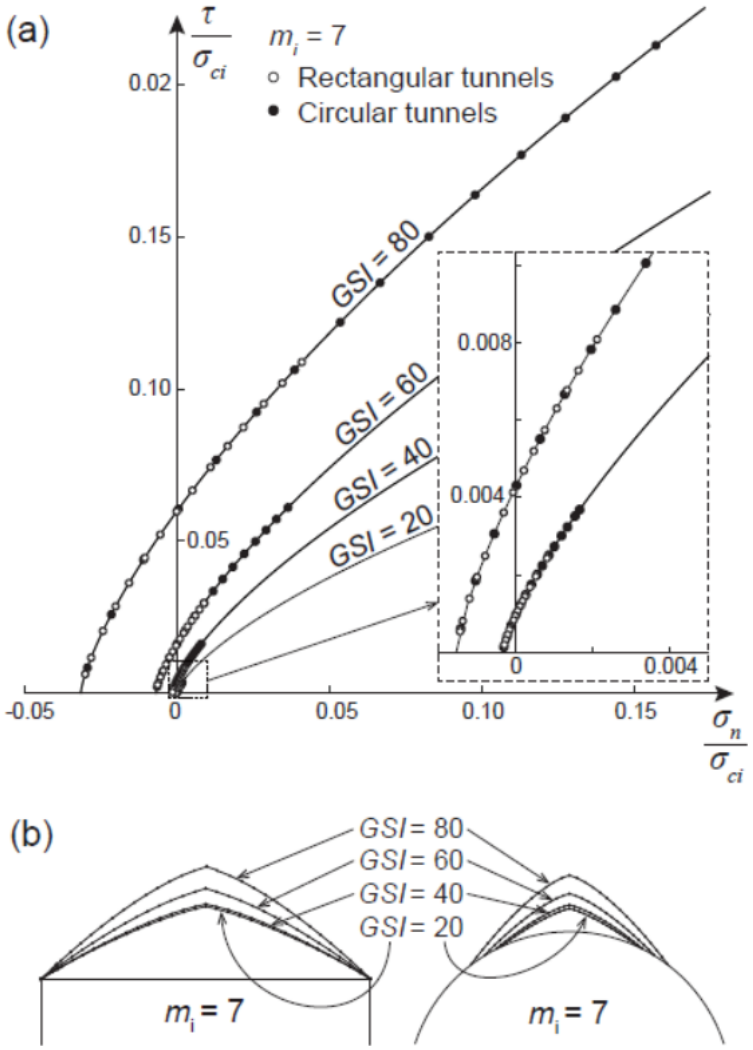
(a)
τ / σci
mi = 7
Rectangular tunnels
Circular tunnels
GSI = 80
GSI = 60
GSI = 40
GSI = 20
0.02
0.15
0.10
0.05
0.008
0.004
0
0.004
-0.05
0
0.05
0.10
0.15
σn / σci
(b)
GSI = 80
GSI = 60
GSI = 40
GSI = 20
mi = 7
mi = 7

Figure 10

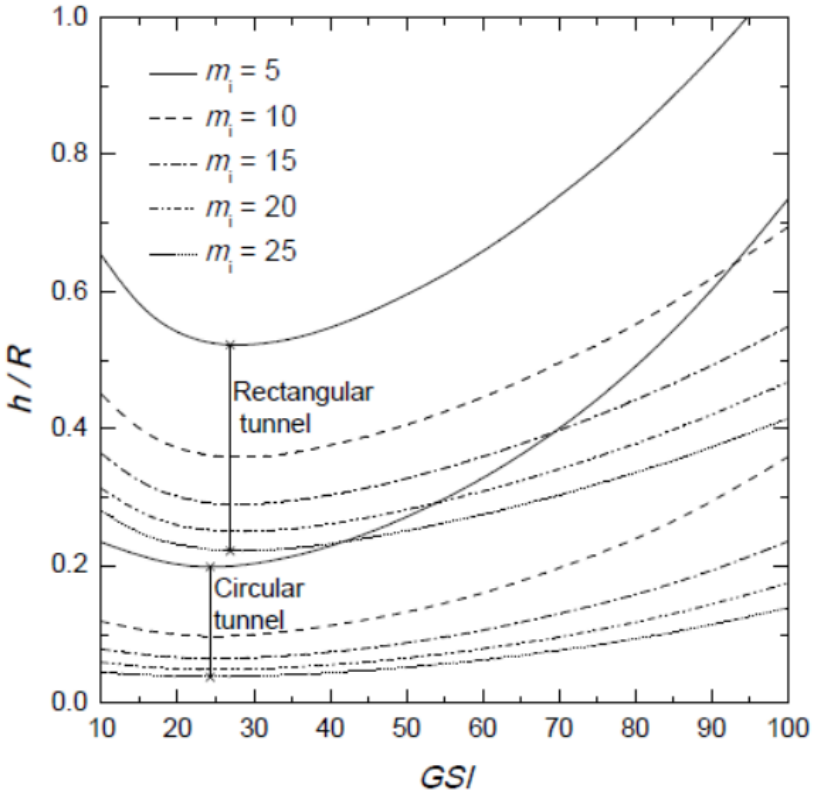
1.0
0.8
0.6
0.4
0.2
0.0
h / R
10
20
30
40
50
60
70
80
90
100
GSI
m_i = 5
m_i = 10
m_i = 15
m_i = 20
m_i = 25
Rectangular tunnel
Circular tunnel

Figure 11

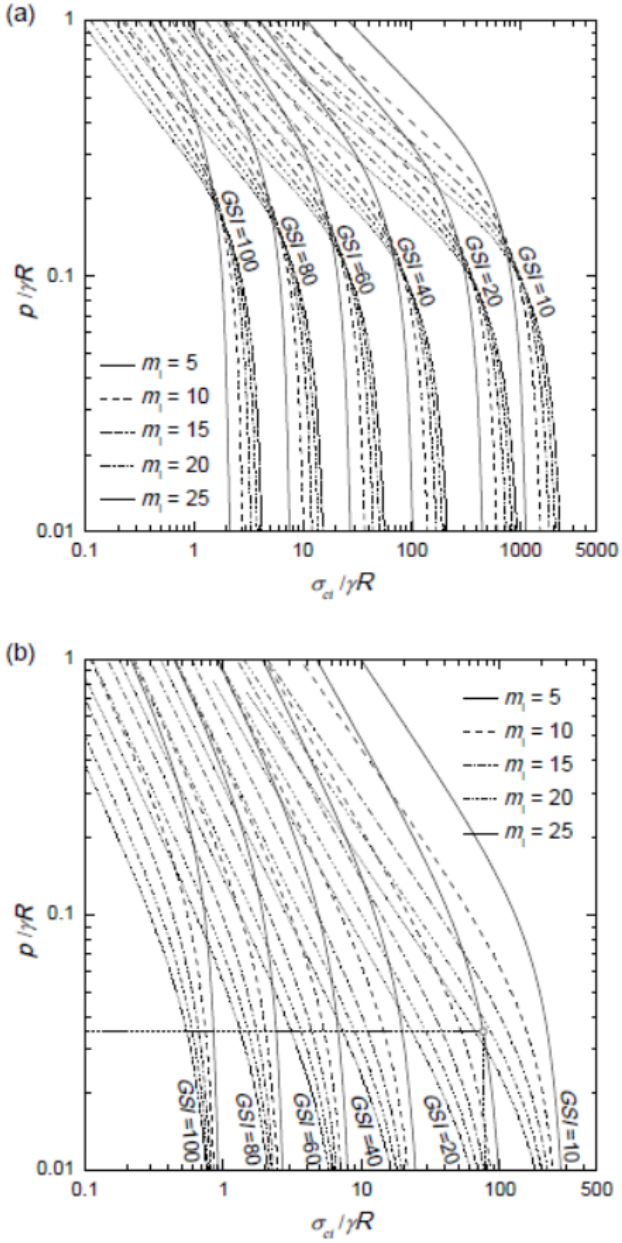
(a)
1
0.1
0.01
p /γR
0.1
1
10
100
1000
5000
σci /γR
GSI=100
GSI=80
GSI=60
GSI=40
GSI=20
GSI=10
mi = 5
mi = 10
mi = 15
mi = 20
mi = 25
(b)
1
0.1
0.01
p /γR
0.1
1
10
100
500
σci /γR
GSI=100
GSI=80
GSI=60
GSI=40
GSI=20
GSI=10
mi = 5
mi = 10
mi = 15
mi = 20
mi = 25

Figure 12

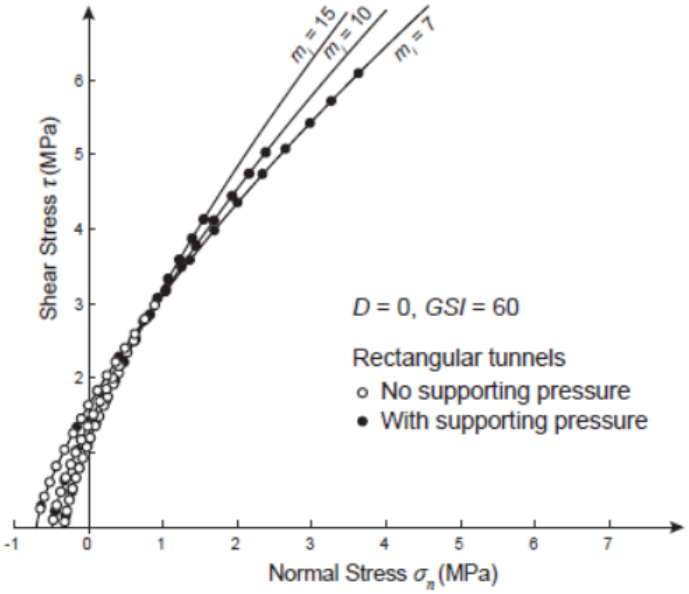
m_i = 15
m_i = 10
m_i = 7
Shear Stress τ (MPa)
Normal Stress σ_n (MPa)
D = 0, GSI = 60
Rectangular tunnels
No supporting pressure
With supporting pressure
-1
0
1
2
3
4
5
6
7

Figure 13

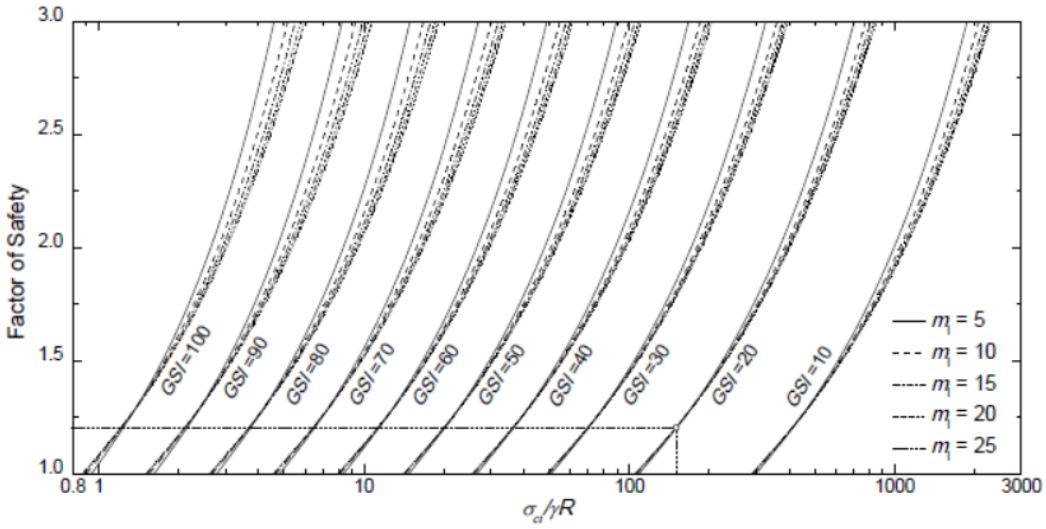
Factor of Safety
3.0
2.5
2.0
1.5
1.0
0.8
1
10
100
1000
3000
$\sigma_c/\gamma R$
GSI =100
GSI =90
GSI =80
GSI =70
GSI =60
GSI =50
GSI =40
GSI =30
GSI =20
GSI =10
m_i = 5
m_i = 10
m_i = 15
m_i = 20
m_i = 25

Figure 14

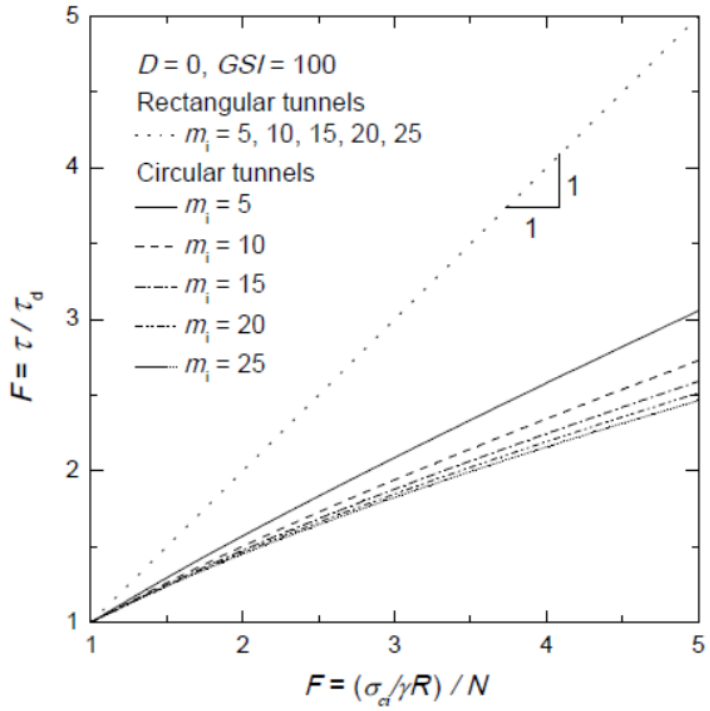
D = 0, GSI = 100
Rectangular tunnels
m_i = 5, 10, 15, 20, 25
Circular tunnels
m_i = 5
m_i = 10
m_i = 15
m_i = 20
m_i = 25
1
1
F = τ / τ_d
F = (σ_d/γR) / N
1
2
3
4
5

Figure 15